Sustainable Energy & Fuels

ROYAL SOCIETY OF CHEMISTRY

PAPER

View Article Online
View Journal | View Issue

Cite this: *Sustainable Energy Fuels*, 2024, **8**, 1314

Investigating the impact of a newly developed chemical modification technique on improving the tribological properties of high oleic soybean oil†‡

Piash Bhowmik,[a] Brajendra K. Sharma,[b] Majher I. Sarker,[b] Hyunsuk Choi,[a] Clement Tang[a] and Sougata Roy *[c]

Soybean oil is currently being studied as lubricating oils in various industries, including automotive, aerospace, and UAV, due to its renewability, biodegradability, and non-toxicity. In vegetable oils, the vast majority of fatty acids are unsaturated. This research demonstrates that the tribological properties of high oleic soybean oil (HOSO) can be improved by the conversion of the unsaturated fatty acids to saturated fatty acids *via* a novel chemical modification process. Ethylaluminum sesquichloride ($Et_3Al_2Cl_3$) and isopropyl bromide were added to a HOSO solution in methylene chloride for chemical modification of the base oil. After stirring and characterization *via* thin layer chromatography (TLC), the organic phase was washed with hydrochloric acid, water, and brine solution. Gas chromatography-mass spectrometry (GCMS), 1D nuclear magnetic resonance (NMR) spectrometry, and 2D heteronuclear single quantum coherence (HSQC) NMR were leveraged to characterize raw and chemically modified soybean oils. The physicochemical properties of high oleic soybean oil (HOSO), chemically modified branched high oleic soybean oil (BHOSO), and high oleic sunflower oil (HOSuO) were determined and correlated with their tribological behavior. The reciprocating friction and wear performance of select lubricants were tested using a ball-on-flat type reciprocating tribometer at room temperature and 100 °C. It was found that the chemical modification process increased wear resistance by around 10% at room temperature and 100 °C. Major differences in wear mechanisms were further analyzed using white light interferometry, scanning electron microscopy (SEM) and energy dispersive X-ray spectroscopy (EDS) techniques.

Received 28th November 2023
Accepted 3rd February 2024

DOI: 10.1039/d3se01526b

rsc.li/sustainable-energy

1. Introduction

Lubricating oils are used in mechanical systems to lower the friction and wear caused by the interaction of moving parts.[1] They are commonly used in the automotive, aerospace, UAV, manufacturing, and hydraulics sectors. Lubricating oil also prevents rust and corrosion, keeping surfaces clean by carrying away dirt and other contaminants.[2] In the majority of sectors till date, mineral oil-based lubricants are being used due to good lubrication properties, wide availability, and chemical stability. Due to toxicity, non-renewability, and non-biodegradability, alternative petroleum oils are being explored quite rapidly from the past decade.[3,4] Lubricating oils that are derived from mineral oil are not environmentally friendly and can pose a threat to the ecosystem if not disposed of correctly.[5,6] Recent research reveals that approximately half of the lubricants utilized worldwide ultimately find their way into the environment as a result of various factors such as usage, accidental spills, evaporation, or incorrect disposal methods.[7] The non-renewable nature of mineral oils leads to their depletion. There is an increasing focus on reducing the environmental impact by minimizing the global dependency on petroleum-based oils.

Environmental regulations have become stricter with a growing concern about the world's limited fossil fuel reserves.[8] As a result, the demand and market for bio-based lubricants has been steadily increasing. Bio-based lubricants are widely utilized in a variety of applications such as mining, dredging, fishing, forestry, and agriculture hydraulic systems.[9–12] Efforts are underway by policymakers and the automobile industry to promote electric vehicles (EVs) as a cleaner alternative. However, even electric vehicles currently rely on petroleum-based lubricating oils especially to lubricate drivetrains. Bio-based lubricating oils for EVs are being actively

[a]*Department of Mechanical Engineering, University of North Dakota, Grand Forks, ND, USA*

[b]*Sustainable Biofuels and Coproducts Research, USDA-ARS-NEA-ERRC, Wyndmoor, PA, USA*

[c]*Department of Mechanical Engineering, Iowa State University, Ames, IA, USA. E-mail: sroy@iastate.edu*

† Mention of trade names or commercial products in this article is solely for the purpose of providing specific information and does not imply recommendation or endorsement by the U.S. Department of Agriculture (USDA). The USDA is an equal opportunity provider and employer.

‡ Electronic supplementary information (ESI) available. See DOI: https://doi.org/10.1039/d3se01526b

explored to support the production of fully eco-friendly cars. Bio-based oils such as vegetable or animal fat oils are good alternate sources for the base oils of the lubricating oil.[13,14] The non-toxicity and biodegradability of bio-based lubricants are their key benefits. In addition to their high molecular weight triglyceride structure fatty acids, vegetable oils exhibit low volatility and a limited range of viscosity changes based on temperature fluctuations. Polar ester groups of vegetable oils have high boundary lubrication capabilities because of their interaction with metal surfaces.[12] Bio-based lubricants have a number of advantages, such as they are made from agricultural products that can be recycled easily, which greatly enhances farmers' income and the rural economy.

In comparison to mineral oils, vegetable oils tend to have inferior tribological properties.[15,16] This is primarily due to the lower levels of oxidation resistance, thermal stability, hydrolytic stability, and poor performance under low-temperature conditions, including cold flow properties. The bis-allylic protons are primarily responsible for poor oxidative stability; these protons are called "bis" because they are adjacent to two double bonds. The vulnerability of vegetable oils to radical attacks results in the generation of polar oxygenated compounds through the process of oxidation.[17–19] This causes deposits that cannot be dissolved and makes oil more acidic and viscous. Due to oxidation, oils' acidity, viscosity, corrosion, and volatility are increased.[12] In contrast, saturated fatty acids have single bonds, which make them less susceptible to oxidation and chemically enhance their stability.[20] Because of the properties and behaviors described above, vegetable oils need to be modified to improve their lubricating properties when used as lubricating oils.

Numerous research investigations have been undertaken to explore the tribological characteristics of bio-based oils, specifically focusing on oils derived from natural sources such as coconut oil,[21] rapeseed oil,[22] jatropha oil,[23] castor oil,[24] canola oil, avocado oil,[25] soybean oil, sunflower oil [26,27] and palm oil.[28] Utilizing waste cooking oil as lubricating oil can be another alternative option since this provides an excellent opportunity to repurpose a material that would otherwise be discarded as waste. However, the major challenges associated with waste cooking oil are maintaining uniform physicochemical properties due to procurement from diverse sources and high cost for filtration and processing to remove the impurities from the base stock.[29,30] Out of the mentioned bio-based oils, soybean oil has a higher global production volume than most other types of vegetable oils.[31] Adhvaryu *et al.*[32] examined the efficacy of different types of soybean oils, including epoxidized soybean oil, with hexadecane as an additive in high-temperature lubricant applications. The study presented the differences in their structural characteristics and oxidative and frictional behaviors, while also discussing the function of a phenolic antioxidant in improving the performance of the lubricants. According to Bihari *et al.*,[33] the addition of ZDDP increased soybean oil's wear resistance by 57% when compared to its pure state, with the possibility of further performance enhancement when coupled with other commercial anti-wear additives. Ameen *et al.*[34] conducted a study on the tribological properties of a mixture of soybean oil and used frying oil FAMEs, which showed good performance as a lubricant candidate under boundary and mixed lubrication conditions, with lower friction coefficients and decreasing specific wear rates with increasing load. Several other researchers have studied the properties of soybean oil and have reported improved tribological properties on modifying the oil or adding various additives or nanoparticles into the oil.[12,35,36]

Efforts are being made globally to enhance bio-based oils as lubricants through techniques like hydrogenation, chemical modifications, and thermal treatments.[37] In a study on rapeseed oil, Ravasio *et al.*[38] investigated various copper catalysts for hydrogenation and found that specific catalysts and preparation methods produced oils with exceptional oxidation stability. Shomchoam *et al.*[39] examined the partial hydrogenation of palm oil using Pd/γ-Al_2O_3 catalysts, resulting in increased oxidation stability from 13.8 to 22.8 h under optimal reaction conditions. Adhvaryu *et al.*[35] examined the tribological properties of chemically and thermally modified soybean oils. Their findings indicate that the chemically modified oils exhibited better friction and wear resistance compared to thermally modified and raw soybean oils. Yosief *et al.*[13] explored the possibility of using chicken fat as a renewable resource for bio-lubricants by chemically modifying it with an isopropyl group using ethylaluminum sesquichloride and found that the modified chicken fat had better tribological and physicochemical characteristics as well as greater oxidative stability. The same research group explored the possibility of using beef tallow as a bio-lubricant and found that alkylating the unsaturated fatty acid chain with isopropyl groups improved its physicochemical properties, including better oxidative stability and low-temperature properties, and higher solubility and density, compared to regular beef tallow.[41] Despite the extensive research and development efforts focused on using soybean oil as a lubricating oil, there is currently no established method available for enhancing its overall operating performance.

In this study, the chemical modification of HOSO into BHOSO was achieved by reacting its double bonds with isopropyl bromide. The reaction was facilitated by utilizing ethyl aluminum sesquichloride ($Et_3Al_2Cl_3$) as the catalyst. Isopropyl bromide (also known as 2-bromopropane) reacts with double bonds through an electrophilic addition reaction. Isopropyl bromide can be added across the double bonds of an alkene using a Lewis acid as a catalyst. The mechanism involves the formation of a carbocation intermediate, which is generated by the attack of the Lewis acid catalyst on isopropyl bromide. The carbocation intermediate can then attack the electron-rich double bond of the alkene, resulting in the formation of a new carbon–carbon single bond. The double bonds in high oleic soybean oil (HOSO) were chemically modified to single bonds (iso-propylation), leading to increased oxidative stability due to the greater stability of saturated carbon bonds. Finally, the physicochemical and tribological properties of BHOSO were investigated in detail and compared against those of HOSO and HOSuO to validate the efficacy of the novel chemical modification process in developing next generation soybean oil-based lubricants.

2. Experimental procedure

2.1 Materials

The HOSO and HOSuO used in this study were received from CHS Inc. (Minnesota, USA) and Columbus Foods Company (Illinois, USA) respectively. HOSuO was chosen as a baseline reference due to its extensive applications in various industries and the similarities it shares with the oil investigated in this study. The GC-MS analysis was used to determine the fatty acid composition of the oils, and the results are presented in Table 1. Hybrid bearings, often found in electric vehicles, use ceramic balls and steel rings to improve their performance. Ceramic balls in bearings are used in electric vehicles because the rotation of the motor can produce shaft current and voltage, which causes electrochemical corrosion in conventional motor bearings and ultimately leads to surface damage.[42] AISI 52100 steel was used as a flat for friction and wear tests, which is widely used to manufacture bearing elements.[43] Silicon nitride balls were used as a counter material for the AISI 52100 flat; both purchased from McMaster-Carr. Hybrid ceramic ball bearings possess outstanding qualities such as effective electrical insulation, high speed capacity, low friction coefficient, and durability against wear.[44] When compared to traditional steel bearings, silicon nitride bearings offer a major advantage in terms of rolling contact fatigue life. It has been demonstrated that silicon nitride ball bearings operating with boundary or mixed lubrication can produce noticeable performance benefits.[45]

2.2 Synthesis of branched high oleic soybean oil (BHOSO)

Unsaturated fatty acids are more prone to oxidation, which can lead to the formation of undesirable compounds and cause the oil to spoil. Isopropylation, a modification technique, can be used to convert the double bonds present in unsaturated fatty acids into single bonds. There are various benefits to following the chosen reaction plan for modifying HOSO. For example, it is a proven method of isopropylation of natural triglycerides.[13,41,46] The utilized chemical reaction scheme is a one-step synthesis to produce the modified oil, making the overall process cost-effective. Additionally, the employed synthetic pathway has resulted in a high yield of products of above 90%. The synthesis of isopropyl branched HOSO (BHOSO) from HOSO is shown in Fig. 1. The HOSO (70 g, ~0.08 mol) was dissolved in methylene chloride in a round-bottomed flask. The flask was sealed by using septa and placed in an ice bath. After that, argon gas was flushed through it. Next, ethylaluminum sesquichloride ($Et_3Al_2Cl_3$) (71.8 g, 0.29 mole) was added slowly over a period of 30 minutes, followed by the addition of isopropyl bromide (35.7 g, 0.29 mole). After stirring the reaction mixture in an ice bath for one hour, it was then allowed to reach room temperature and stirred overnight in an argon environment. Thin layer chromatography (TLC) was employed to verify the completion of the reaction. Next, the reaction mixture was mixed with 100 mL of ethylacetate. Approximately 10 mL of 10% hydrochloric acid (HCl) was added slowly until the formation of clear aqueous and organic phases was observed. By this acid treatment the residue of the catalyst ($Et_3Al_2Cl_3$) was neutralized and became aqueous soluble. To completely remove the residue, around 150 mL of water was used each time to wash the organic layer three times, and then about 150 mL of brine solution was used to wash it once. Sodium sulfate was added to remove any remaining water from the organic phase, and then ethyl acetate was evaporated off using a rotary evaporator. The reaction resulted in a yield of 91% based on the initial quantity of HOSO used.

Table 1 Fatty acid composition of HOSO and HOSuO

	Palmitic acid	Stearic acid	Oleic acid	Linoleic acid
HOSO	4.7%	2.3%	89.3%	**3.8%**
HOSuO	3.8%	2.1%	85.2%	**8.9%**

2.3 Nuclear magnetic resonance (NMR)

The samples were analyzed using a 14 Tesla NMR spectrometer from Agilent Technologies located in Santa Clara, CA. The spectrometer is equipped with a 5 mm One NMR probe. All samples were dissolved in deuterated chloroform from Cambridge Isotopes Laboratories in Andover, MA and analyzed at 25 °C. A relaxation delay of 2 seconds and an acquisition time of 2.28 seconds, along with a 45° pulse angle were used to acquire the ^{1}H spectra. The spectral width of the ^{1}H spectra was 12 parts per million (ppm). The ^{13}C spectra were obtained by averaging 1000 transients using a 45° pulse angle, a 2 second relaxation

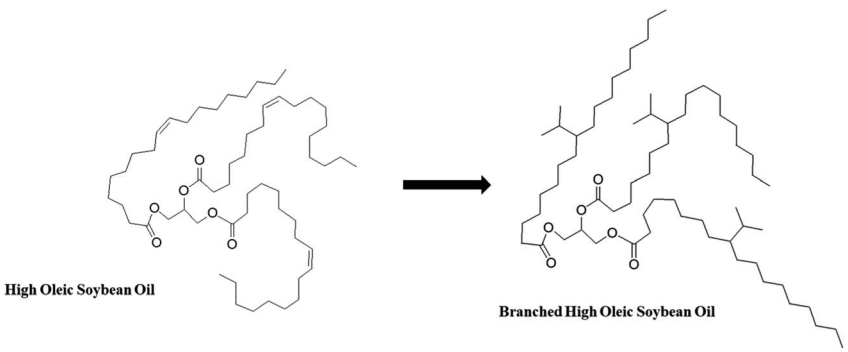

Fig. 1 Isopropylation of HOSO with an isopropyl group using $Et_3Al_2Cl_3$.

delay, and a 0.87 second acquisition time. These spectra had spectral widths of 253 ppm. The direct C–H correlations were established in select species by gradient-selected, multiplicity-sensitive 2D-HSQC (heteronuclear single quantum coherence spectroscopy) using adiabatic pulses in which the 32 directly detected transients (2k points) were averaged for 200 indirectly detected increments. The spectral widths in the direct dimension are 12 ppm and 200 ppm in the indirect dimension. For all the spectra, residual solvent resonances were utilized as internal chemical shift references. The spectra were processed using SpinWorks4 software (v4.2.10), developed by Kirk Marat at the University of Manitoba, Canada.

2.4 Gas chromatography-mass spectroscopy (GC-MS)

In order to determine the fatty acid composition of the starting materials and products, namely HOSO and BHOSO, a gas chromatograph (model 8890N) manufactured by Agilent Technologies was employed. The gas chromatograph utilized in the analysis was equipped with an Agilent model 5977N mass selective (MS) detector. Additionally, a Supelco SP-2380 column measuring 30 m in length, 0.25 mm in diameter, and featuring a film thickness of 0.2 μm was also utilized. For GC-MS analysis, the starting materials HOSO and BHOSO were transesterified to form fatty acid methyl esters (FAMEs). Approximately 100 mg of HOSO or BHOSO was added to 20 mL reaction vials. Then 15 mL of 2% sulfuric acid (H_2SO_4) in methanol was added. After capping the reaction vials, they were stirred for 2 hours at 80 °C. The reaction mixture was allowed to cool down to room temperature (RT), and the methanol in the mixture was evaporated under vacuum. The resulting mixture was then subjected to an extraction process using ethyl acetate to extract the desired FAMEs. The crude product was washed thrice with 15 mL of water to eliminate any traces of glycerol and the acid catalyst from the FAMEs. The ethyl acetate extract containing the fatty acid methyl esters (FAMEs) was further processed by washing it with 5 mL brine solution. Afterwards, the extract was dried using anhydrous sodium sulfate (Na_2SO_4). 5 μL of the ethyl acetate extract was diluted with 1 mL of ethyl acetate before injection into the GC-MS to prepare the samples for GC-MS analysis. The column was initially heated to 70 °C and held at this temperature for 2 minutes. Subsequently, the temperature of the column was ramped up to 250 °C at a rate of 20 °C per minute. Once the temperature reached 250 °C, it was held steady for 10 minutes. Helium gas was employed as the carrier gas, flowing at a rate of 1.5 mL per minute. A split ratio of 50 : 1 was used. The injector temperature was set to 230 °C while the detector temperature was maintained at 280 °C.

2.5 Pressure differential scanning calorimetry (PDSC)

DSC thermograms of the test samples were recorded using a TA Instruments Q20 instrument from New Castle, DE, USA. In the experimental procedure, approximately 1.5–2.0 mg of the sample was precisely weighed into an aluminum pan. To facilitate the interaction of the sample with the reactant gas (dry air), the pan was sealed using pinhole lids. Through the utilization of controlled gas diffusion *via* a pinhole, the interaction between the sample and the reactant gas (dry air) allowed for the saturation of the oil sample with air while effectively preventing its volatilization. The oil-film thickness in the pan must be less than 1 mm to achieve effective oil/air interaction and remove any disparity in the result caused by gas diffusion limits. The temperature calibration of PDSC was conducted using the melting point of indium metal (156.6 °C) at a heating rate of 10 °C min^{-1}. The sample pan was then loaded into a PDSC cell, which was then sealed and charged with dry air at 200 psi (1378.95 kPa). Data were collected while the cell temperature was increased from room temperature to 300 °C at a rate of 10 °C min^{-1}. Heat flow (W g^{-1}) *versus* temperature plots were utilized for the determination of the oxidation onset temperature (OT, °C) and signal maxima temperature (SM, °C) using the provided software. Each sample was subjected to three separate tests, and the average results, rounded to the nearest tenth of a degree, are reported.

2.6 Viscosity, density, and viscosity index analysis

An SVM3001/G2 viscometer with an Xsample 530 automatic sample changer (Anton Paar GmbH, Graz, Austria) was used to test the dynamic viscosity and densities of biobased oils at 40 °C and 100 °C in accordance with ASTM D7042 (ref. 47) and ASTM D4052 (ref. 48) respectively. The process involved transferring 20 mL of each sample into a vial and placing it in the carousel of the automated sample changer. The device automatically determines and displays the kinematic viscosity at 40 °C and 100 °C by utilizing the measured dynamic viscosity and density values at those specific temperatures. Following the ASTM D2270 standard, the viscosity index (VI) of biobased oils was then determined automatically using the kinematic viscosity data at 40 °C and 100 °C.[49]

2.7 Cloud point (CP)

The cloud point was determined following the guidelines of ASTM D5773 on Phase Technology PSA-70X model automatic cloud/pour/free apparatus. Prior to analysis, the samples were maintained in the laboratory at a room temperature of 22 ± 1 °C. An aliquot of the sample, 0.150 ± 0.005 mL was then added to a chamber inside the instrument with a reflective surface on the bottom, which was then sealed. A vacuum applied to the closed chamber removes ambient moisture. The samples were then cooled at a rate of 1.5 ± 0.1 °C per minute. The inside of the chamber was continuously illuminated by using an internal light source directed onto the sample at an angle and continuously monitored by an optical detector located directly above the sample. In the liquid form, the light source went through the sample and reflected off the bottom of the chamber. As the sample cools and crystals begin to form, these cause the directed light to scatter, some being directed to the optical sensor directly above the sample. The formation of crystals, known as the cloud point, was determined by observing the sample temperature at which directed light was deflected onto the optical sensor. The determined applicable temperature range for this method was −60 to 49 °C.

2.8 Pour point (PP)

Analysis of the pour point D5949 took place immediately after the determination of cloud point D5773. A pulse of dry air was applied to the sample. When this occurred, a change in optical scattering was observed by the optical sensor. The sample was cooled at the same rate of 1.5 °C per minute, with pulses of dry air applied at every 3 °C. When the sample was frozen, there was no noticeable change in the optical response. The previous reading was then denoted as the pour point. For example, if no optical change is observed upon the application of a dry air pulse at −27 °C, then the pour point is recorded as −24 °C. The determined range for this method was −57 °C to 51 °C.

2.9 Reciprocating friction and wear tests

The tribological characteristics of the vegetable oils were evaluated by performing friction and wear tests using a reciprocating ball-on-flat contact setup. These tests were performed on an Rtec MFT2000 tribometer (Make: Rtec Instruments, USA). For the tribo-pair, AISI 52100 steel was used as the flat surface, and silicon nitride (Si_3N_4) balls (6 mm diameter) were utilized as the counter material. The steel samples were polished to achieve an average surface roughness (R_a) of less than 0.1 μm. The surface roughness was measured using a Profilm 3D white light profilometer (Make: KLA Instruments, USA). The experiments were conducted using a force of 75N, which resulted in a maximum Hertzian contact pressure of 2.7 GPa. The sliding velocity and total sliding distance for each tribo-test was 0.1 m s^{-1} and 500 m respectively at room and elevated (100 °C) temperatures. Each experiment was repeated three times to establish the statistical significance of the test results. Fig. 2 illustrates the schematic representation of the experimental setup for the tribological tests, including the lubricant and sample holder. After the experiment, a white light interferometer was used to analyze wear volume and wear depth for each tribotest. Major wear mechanisms were analyzed using scanning electron microscopy (SEM) and energy dispersive X-ray spectroscopy (EDS). SEM imaging was conducted using a Quanta FEG 650 model (make: FEI Inc., USA) while EDS analysis was performed using a Bruker Nano XFlash SUE 6 system equipped with Bruker Quantax software (make: Bruker Inc. USA).

3.1 Experimental analysis of raw and formulated lubricants

3.1.1 NMR analysis. Proton and carbon NMR analysis clearly indicated the presence of isopropyl (iPr) groups in the BHOSO triglyceride molecule as shown in Fig. 3 and 4 (bottom line).

In Fig. 3 (bottom red line), the doublet peak at 0.78 ppm corresponds to the $-CH_3$ protons of the isopropyl (i-Pr) groups in BHOSO which is missing in the HOSO proton spectrum (Fig. 3, top blue line). The –CH– from the i-Pr group appears at 1.65 ppm as a multiplet. The multiplets at 1.02 and 1.09 ppm correspond to the –CH-i-Pr group and its next $-CH_2$ protons, respectively. From the peak area integration of the $-CH_3$ protons, the number of i-Pr groups in a BHOSO molecule is calculated to be 13.9/6 = 2.32 i-Pr groups/triglyceride. A similar number (2.37) is also shown by the area of the –CH– proton of the i-Pr group. Peaks representing the allylic (1.98 ppm) and vinylic protons (5.32 ppm) are shown in the HOSO spectrum but are not visible in BHOSO confirming that the double bonds were alkylated. Three peaks at 4.12, 4.26 and 5.23 ppm are common in both BHOSO and HOSO spectra (Fig. 3) which represent the protons of the glycerol backbone confirming that the backbone remains intact in BHOSO after the alkylation reaction.

The ^{13}C spectrum of the BHOSO (Fig. 4, bottom red line) shows peaks at 19.1 ppm, 27.7 ppm and 43.6 ppm which correspond to the carbons of the isopropyl group. The common peaks at 61.9 and 68.7 ppm in both HOSO and BHOSO spectra represent the carbons of the glycerol backbone. The carbonyl carbons of BHOSO are represented by the peaks at 172.5–173.0 ppm.

HSQC shows (Fig. 5) that the $-CH_3$ from the i-Pr group (0.78 ppm) is connected to the 19.1 ppm ^{13}C spectrum. The –CH– from the i-Pr group which appears at 1.65 ppm is connected to 27.7 ppm ^{13}C in the HSQC spectrum. The multiplet at 1.02 ppm represents the –CH–i-Pr group and it is connected to the 43.6 ppm ^{13}C in the HSQC spectrum.

3.1.2 GC-MS analysis. GC-MS data show that FAMEs from HOSO (Fig. 6, red line) contain 4.7% methyl (Me) palmitate ($C_{17}H_{34}O_2$), 2.3% Me-stearate ($C_{19}H_{38}O_2$), 89.3% Me-oleate ($C_{19}H_{36}O_2$) and 3.8% Me-linoleate ($C_{19}H_{34}O_2$). As a result of chemical modification, most of the oleic acid chains of HOSO are

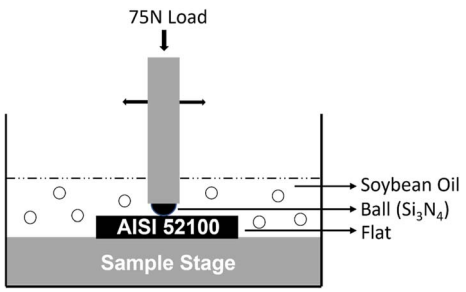

Fig. 2 Schematic diagram of the tribological experimental setup.

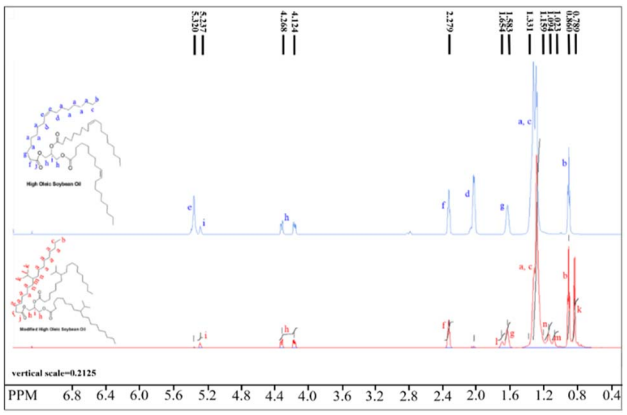

Fig. 3 Comparison between the ^1H NMR spectra of HOSO (top blue line) and BHOSO (bottom red line). Spectral peaks are assigned with their corresponding protons in letters.

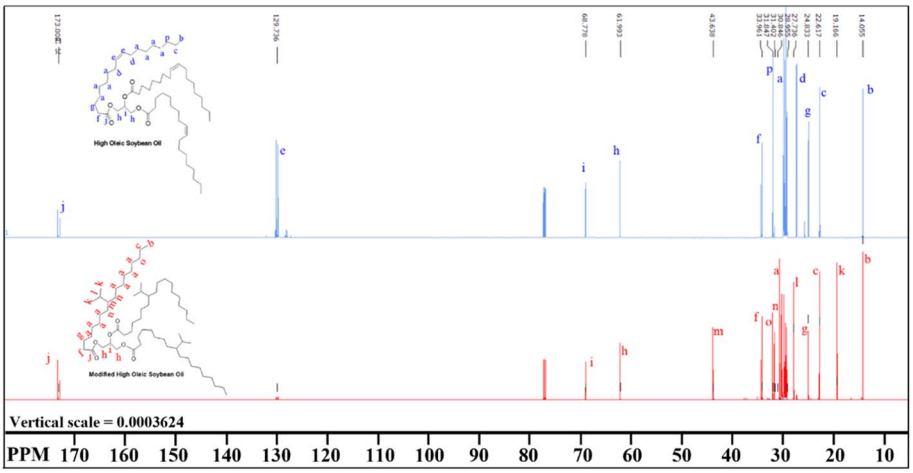

Fig. 4 Comparison between the ^{13}C NMR spectra of the HOSO (top blue line) and BHOSO (bottom red line). Spectral peaks are assigned with their corresponding carbons in letters.

branched with isopropyl groups to form i-Pr branched methyl stearate ($C_{22}H_{44}O_2$, MW 340). The FAME composition of the synthesized BHOSO is determined by the GC-MS analysis (Fig. 6, black line) and includes 6.3% of Me-palmitate, 2.8% Me-stearate, 2.5% Me-oleate, 2.1% Me-linoleate and 86.3% i-Pr branched Me-stearate. The peak representing i-Pr branched Me-stearate ([M+] = 340 m/z) appears at 10.9 min retention time, which is mainly produced from 89.3% of Me-oleate (appears at 10.3 min on the spectrum) in HOSO during chemical modification.

3.2. Physicochemical properties of the HOSO, BHOSO and HOSuO

HOSO was selected for this study because of its stability since this oil is combined with tocopherol.[50] Tocopherol functions as an antioxidant that helps to prevent oxidation by scavenging free radicals.[51]

3.2.1. Density. The influence of introducing branching into HOSO on density was examined at 40 °C and 100 °C, as displayed in Table 2. The introduction of the isopropyl group into the HOSO led to a slight decrease in density at all the tested

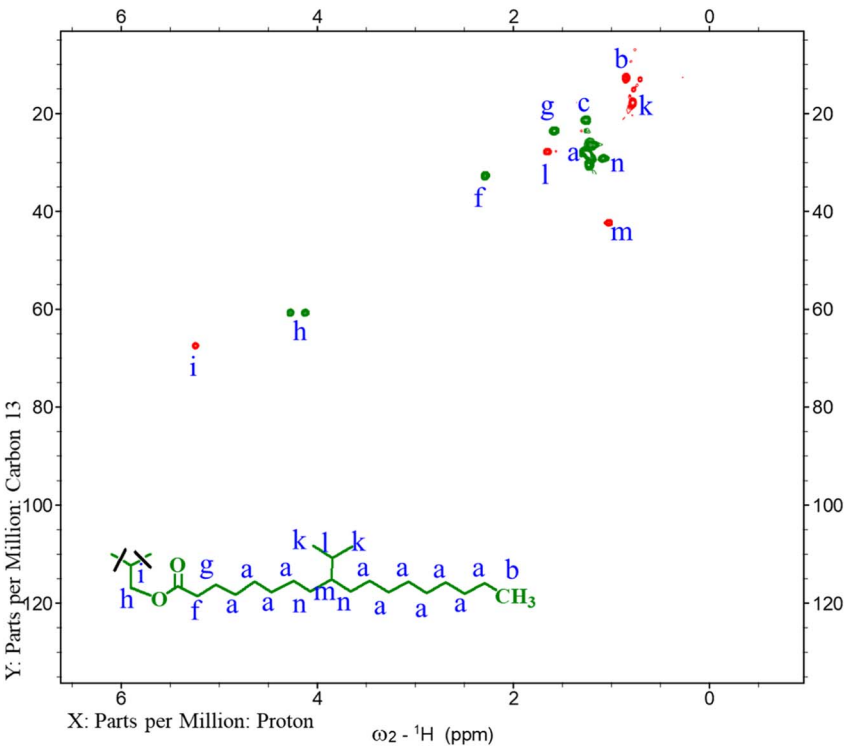

Fig. 5 HSQC NMR spectra of BHOSO, showing connections between peaks associated with the i-Pr branch.

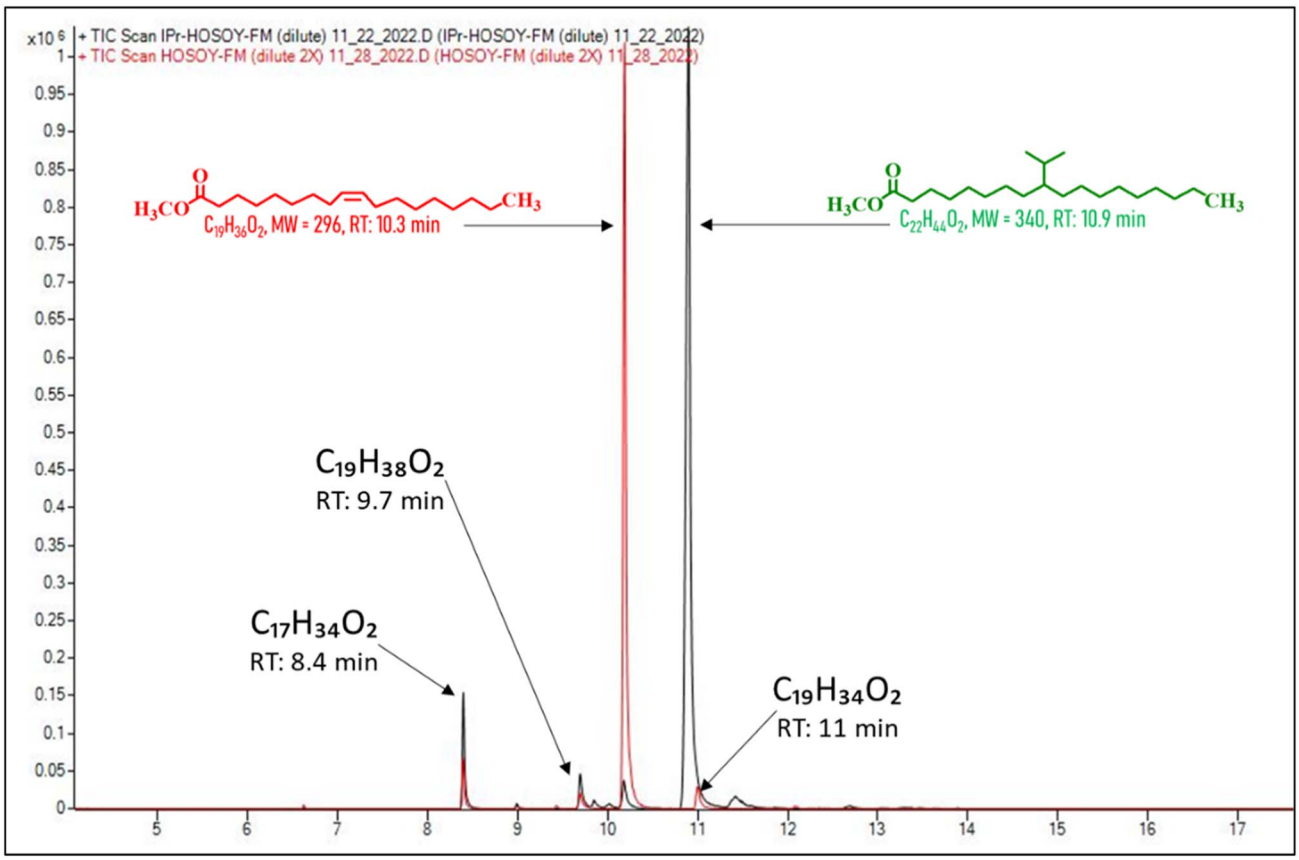

Fig. 6 GC-MS-total ion count *vs.* retention time for FAMEs of HOSO (red line) and BHOSO (black line). The peaks are annotated with the FAME chemical formula: methyl palmitate ($C_{17}H_{34}O_2$, MW: 270); methyl stearate ($C_{19}H_{38}O_2$, MW = 298); methyl oleate ($C_{19}H_{36}O_2$, MW = 296); i-Pr branched methyl stearate ($C_{22}H_{44}O_2$, MW = 340).

temperatures. At 40 °C, for example, while the density of HOSO was found to be 0.8993 g cm^{-3}, the density of BHOSO was measured to be 0.8965 g cm^{-3}. The density decreased, possibly because of replacing the double bonds by i-Pr groups.[13] The density of all the oils reduced with increasing temperature.[52] Thermal analysis curves for each lubricant are provided in the ESI (Fig. S1‡).

3.2.2. Kinematic viscosity and viscosity index. Kinematic viscosity refers to a fluid's capacity to resist internal flow when subjected to gravitational forces. The quantification of kinematic viscosity involves measuring the time in seconds for a predefined volume of fluid to flow a certain distance under the influence of gravity within a viscometer that is precisely calibrated for temperature control. In contrast, the viscosity-index (VI) is a parameter that explains how a fluid's thickness alters

Table 2 Comparison of the physicochemical properties of BHOSO with HOSO and HOSuO[a]

	Temperature (°C)	HOSO	BHOSO	HOSuO
Density (g cm^{-3})	40	0.8993	0.8965	0.8999
	100	0.8596	0.8573	0.8603
Kinematic viscosity (mm^2 s^{-1})	40	38.93	142.13	38.93
	100	8.49	19.39	8.49
Dynamic viscosity (mPa s^{-1})	40	35.02	127.42	35.03
	100	7.30	16.62	7.31
Viscosity index		203.6	155.9	204.13
Oxidative onset temp, OT (°C)		202.2	199.2	181.9
Oxidative peak temp, PT (°C)		210.9	213.7	205
Pour point (PP, °C)		−15	−12	−22
Cloud point (CP, °C)		−10.9	−14.5	−8

[a] Each property value represents an average derived from three separate measurements.

with temperature changes. A high VI signifies that a fluid's viscosity is less likely to fluctuate over a wide temperature range, making it more stable in a broad range of temperature conditions. Table 2 provides a comparison of the kinematic viscosity and viscosity index (VI) of HOSO, BHOSO, and HOSuO. At 40 °C, BHOSO exhibits a kinematic viscosity nearly four times higher than that of HOSO. As the temperature increases, the kinematic viscosity of all oils decreases. The viscosity decreases exponentially as the temperature increases.[52] Although the BHOSO maintains a higher kinematic viscosity than the HOSO at elevated temperature, the difference is less significant than that at 40 °C. The elevated viscosity of BHOSO in comparison to HOSO can be attributed to the presence of an alkyl branch, which could impede the flow of molecules and result in a higher kinematic viscosity.[41] Another possible explanation for the higher viscosity of BHOSO is the presence of oligomers in BHOSO.[53] The molecular weight of methyl oleate from HOSO and i-Pr branched methyl stearate from BHOSO are 296 and 340, respectively (refer to Fig. 6). It has been observed previously that viscosity is increased as the molecular weight of a lubricant is increased. Additionally, another study reported a decrease in viscosity as the number of double bonds in the molecule is increased.[54] Table 2 also shows that the BHOSO (VI: 155.9) has a lower viscosity index than the HOSO (VI: 203.6) and the HOSuO (VI: 204.13). The low viscosity index (VI) of BHOSO suggests that its viscosity will undergo comparatively higher changes in response to temperature variations, while the viscosity of HOSO and HOSuO will remain relatively stable.

3.2.3. Oxidation stability. The oxidation stability of BHOSO, HOSO, and HOSuO was examined through PDSC, and the temperatures at which onset oxidation (OT) and peak oxidation (PT) occurred are presented in Table 2. Higher OT and PT values indicate that the substance is more resistant to oxidation. In comparison to HOSO and HOSuO, BHOSO shows a slightly higher PT value, but almost the same OT as HOSO. The oxidation stability of fatty acids is influenced by the degree of unsaturation. Fatty acids with higher degrees of unsaturation exhibit reduced oxidation stability.[55] Compared to HOSO or HOSuO, BHOSO has a slightly higher PT value; this observation can be attributed to the fact that the fatty acid components of the triglycerides contain a lower total number of unsaturated bonds. In addition, the oxidative stability (OT) value of BHOSO may have decreased due to the presence of oligomers in BHOSO.

3.2.4. Cloud point and pour point. The cloud point, commonly referred to as CP, denotes the temperature at which the oil begins to form a cloudy appearance upon cooling, while the temperature beyond which oil will no longer flow is known as the pour point (PP). As can be seen in Table 2, BHOSO exhibited a reduced CP in comparison to HOSO. This finding suggests that the branching of the fatty acid tail group contributed to an improvement in the cold flow characteristics. Introducing branching to the oil can lower its cloud point by preventing close packing during cooling.[56] But compared to HOSuO, both HOSO and BHOSO had a higher pour point. This can be potentially due to a higher polyunsaturation level (linoleic acid 8.9% *vs.* 3.8% in HOSO) in HOSuO compared to HOSO.[40,41,57] Lower pour points are associated with vegetable oils that contain more unsaturated fatty acid chains.[56]

4. Results and discussion

4.1 Analysis of the coefficient of friction

The coefficient of friction (COF) of HOSO, BHOSO, and HOSuO at room temperature and 100 °C was investigated using a ball-on-flat type reciprocating sliding test and plotted against the sliding distance as shown in Fig. 7. BHOSO showed the highest coefficient of friction under both temperature conditions, followed by HOSuO and HOSO. The average COF under HOSO lubricated conditions was measured to be 0.067 ± 0.019 at room temperature and it decreased to 0.059 ± 0.022 at high temperature. For BHOSO, the COF increased by 22.8% as compared to that of HOSO at room temperature. At 100 °C, the COF of BHOSO increased by 18.5% as compared to that of HOSO. The

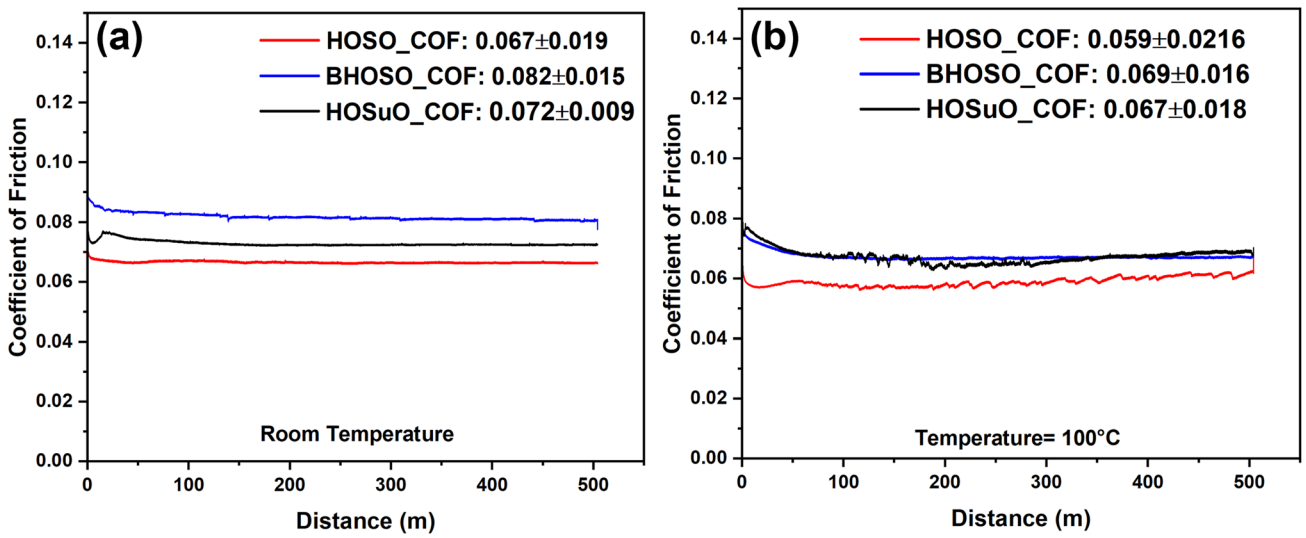

Fig. 7 Coefficient of friction response of the vegetable oils at (a) room temperature and (b) 100 °C.

BHOSO lubricant possesses saturated fatty acids along with branched carbons. Due to the branching of carbons, the coefficient of friction for BHOSO was higher than that of other oils tested under both room temperature and 100 °C testing conditions.[58] The irregular molecular shape can be another potential reason behind the high coefficient of friction, as reported by Bayer *et al.*[59] Other studies correlated the effect of molecular structure with the resulting coefficient of friction.[60,61] The coefficient of friction of HOSuO was higher than that of HOSO under both room temperature and 100 °C test conditions. This can be attributed to the variation in fatty acid composition, as shown in Table 1. Reeves *et al.*[62] noted that there were discrepancies in the COF for various bio-based oils, which can be explained by variations in their individual fatty acid compositions. The lower fraction of oleic acids found in oils provides a higher value of the coefficient of friction. For all tested oils under 100 °C conditions, the coefficient of friction value decreased which is potentially due to the change in physical qualities of oils which occurs under elevated temperature conditions. Attia *et al.*[63] observed physicochemical changes in soybean oil and other bio-based oils due to variation in operating temperature. Zhang *et al.*[58] presented the correlation between the coefficient of friction of different synthetic lubricating oils and different operating temperature conditions. They reported a decreasing trend in COF values as the operating temperature increased. It can be observed from Fig. 7 that the friction curve stabilizes at a sliding distance of around 30 meters under room temperature conditions. However, at 100 °C, stabilization requires a slightly longer distance of around 70 meters. Interestingly, BHOSO exhibited minimal fluctuation in its friction curve at high temperature which can be attributed to the formation of a stable tribofilm due to saturated fatty acids.[64]

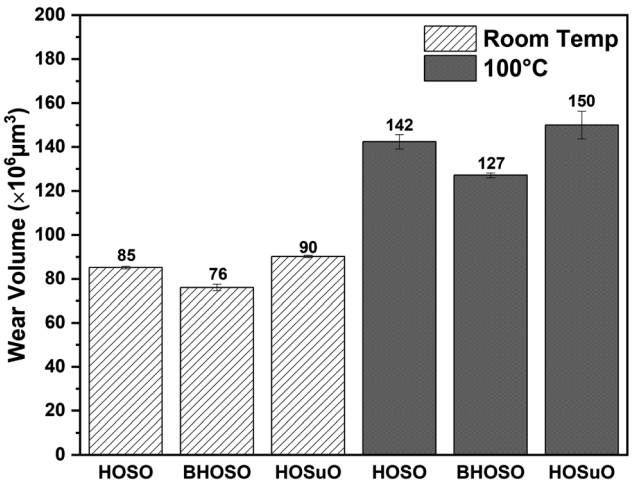

Fig. 8 Wear volumes of the AISI 52100 steel flat samples for different vegetable oils under room temperature and 100 °C conditions.

4.2 Analysis of wear volume

Fig. 8 presents a comparative analysis of wear volumes in flat samples due to tribological tests conducted using different lubricants and at different operating temperatures. The wear volume in the HOSO lubricated case at room temperature was measured to be 85 × 10^6 μm^3 while at high temperature, it increased significantly to 142 × 10^6 μm^3. In contrast, BHOSO presented 10.6% and 10.7% increased wear resistance as compared to HOSO under room temperature and high-temperature conditions, respectively. Less unsaturated fatty acids in BHOSO helped in presenting enhanced wear resistance as compared to that of HOSO. It has been observed that an increase in unsaturation in fatty acids results in decreased wear resistance.[62,64] The average wear volume of HOSuO was slightly higher than that of HOSO at both temperature levels. This can be attributed to the presence of a higher amount of

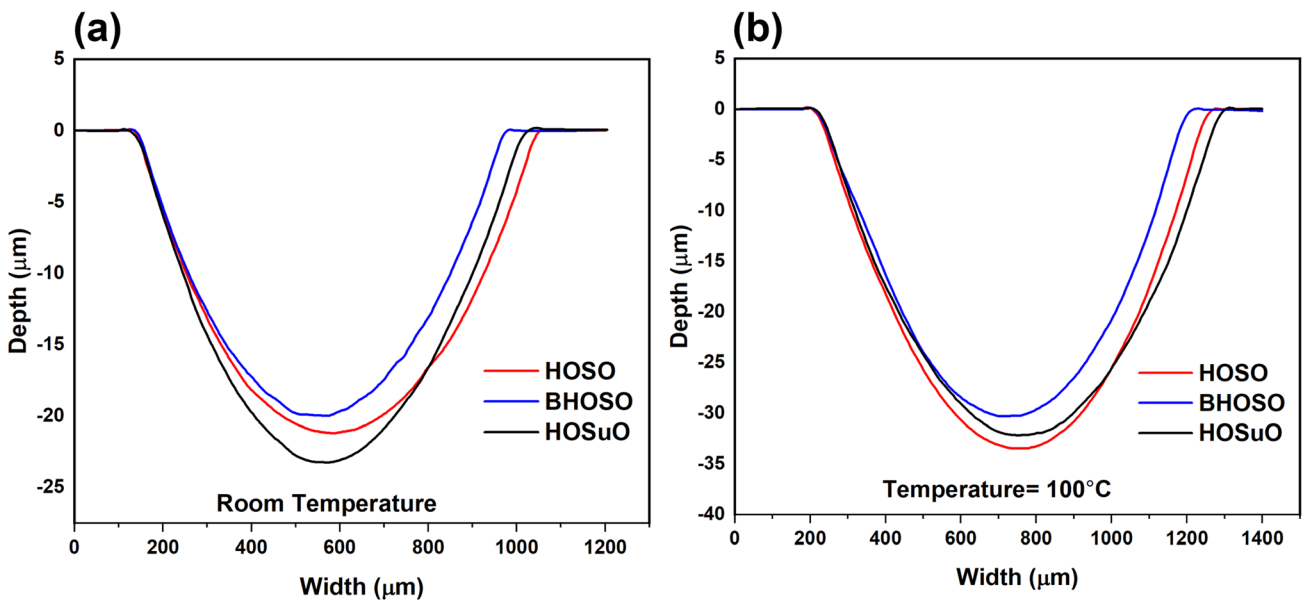

Fig. 9 Two-dimensional depth profiles of wear tracks captured along the transverse direction at (a) room temperature (b) 100 °C.

polyunsaturated fatty acid (linoleic acid) in HOSuO than in HOSO as mentioned in Table 1.[64]

When exposed to high temperatures, all of the lubricants experienced a decrease in wear resistance. This can be due to changes in the physical properties of the oils, which were discussed earlier. 2-dimensional wear depths were measured along the transverse direction. As depicted in Fig. 9, the wear depth value of HOSO and HOSuO were quite similar under both temperature conditions. BHOSO exhibited the lowest wear depth under both operating temperature conditions. The generation of a stable tribofilm by saturated fatty acids can be correlated with decreased wear depths and wear volumes under BHOSO lubricated conditions.[64] Wear volumes in balls were significantly less than that observed in the flats because of extreme wear resistance of ceramic materials as compared to metallic materials. Hence, ball wear volume analysis was excluded in this study.

4.3 Wear mechanisms under room and high temperature test conditions

4.3.1 Tribological condition: flat wear. The wear tracks on the flat samples were analyzed using SEM and EDS techniques to identify the dominant wear mechanism and investigate any potential transfer of material between the flat and ball samples. No material from the ball was transferred to the flat surface as

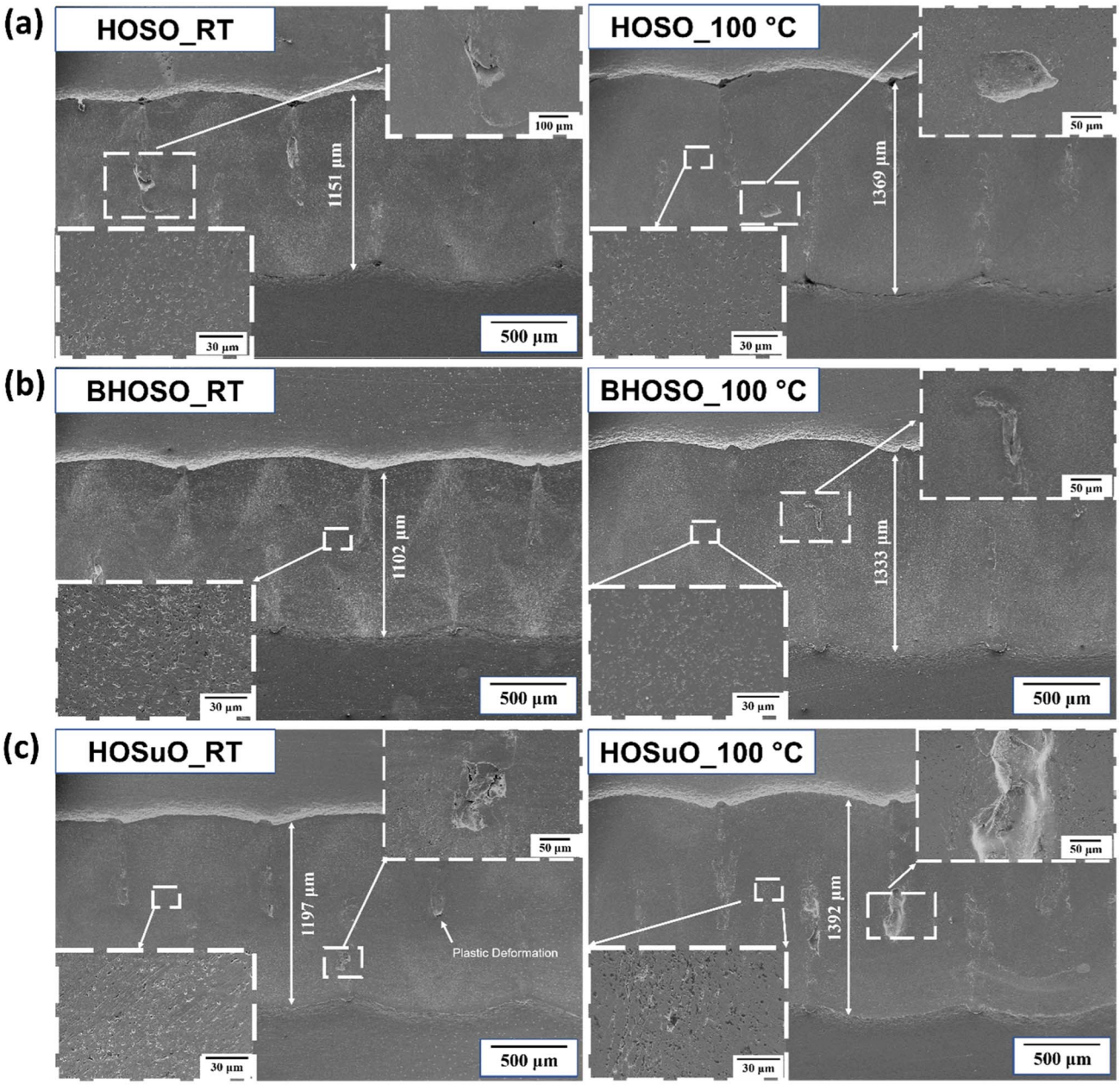

Fig. 10 SEM images of wear tracks on the AISI 52100 samples (a) HOSO, (b) BHOSO and (c) HOSuO at room temperature and 100 °C. Representative images showing the morphology and wear mechanism of the wear tracks after the sliding tests.

confirmed by the EDS analysis of the flat tracks. Abrasive wear was observed to be the primary wear mechanism at room temperature and 100 °C. Abrasive wear is the removal of small particles from one or both surfaces caused by the presence of abrasive particles or materials that are harder than the surface being worn.[65,66] Dislodged metal flakes or spalling was observed when HOSO was used as the lubricant under both room and high temperature conditions (Fig. 10a). Material removal or spalling in a lubricated tribo-test can result due to breakdown of the lubricant film that separated the contacting surfaces. This can be observed as a result of high load, contact pressure, temperature, insufficient lubrication, contamination, or the presence of corrosive or abrasive particles.[67] The size of the flakes was found to be larger under high-temperature conditions, indicating severe degradation of the sample surface at higher temperature. Corrosion-induced pits were observed under both room temperature and high-temperature conditions in all three lubricant cases as shown in the bottom left corner of Fig. 10. However, the pit coverage area inside the track was slightly higher under BHOSO lubricated conditions (Fig. 10b) which could have resulted in a higher friction coefficient in BHOSO lubricated cases (refer Fig. 7). The wear tracks in the BHOSO lubricated case did not show any significant metal flaking at room temperature. However, discrete local region metal flakes were observed at high temperatures, but they were not prevalent throughout the track. BHOSO contained the highest amount of stearic acid which potentially helped in enhancing the wear resistance.[68] The wear track width was found to be the smallest under BHOSO lubricated conditions at both temperature levels. Adhvaryu witnessed a decreased wear track width in the soybean oil, where the molecule's structure was altered chemically.[69] The reduced wear track width is consistent with BHOSO's low wear volume and high wear resistance. HOSuO lubricated samples exhibited the highest amount of dislodged metal flakes as observed in Fig. 10c and this phenomenon was more prominent under high temperature conditions.

4.3.2 Tribological condition: ball wear. Fig. 11 presents the backscattered electron images (BSE) and corresponding elemental mapping on worn out balls under different lubrication conditions. The volume of worn-out regions in balls increased with increasing test temperature which is consistent with earlier observations.[70,71] The worn-out regions on balls are marked with yellow rectangles in Fig. 11 indicating reduction in ball worn out area under BHOSO lubricated conditions. The EDS elemental mapping on balls revealed material transfer (Fe

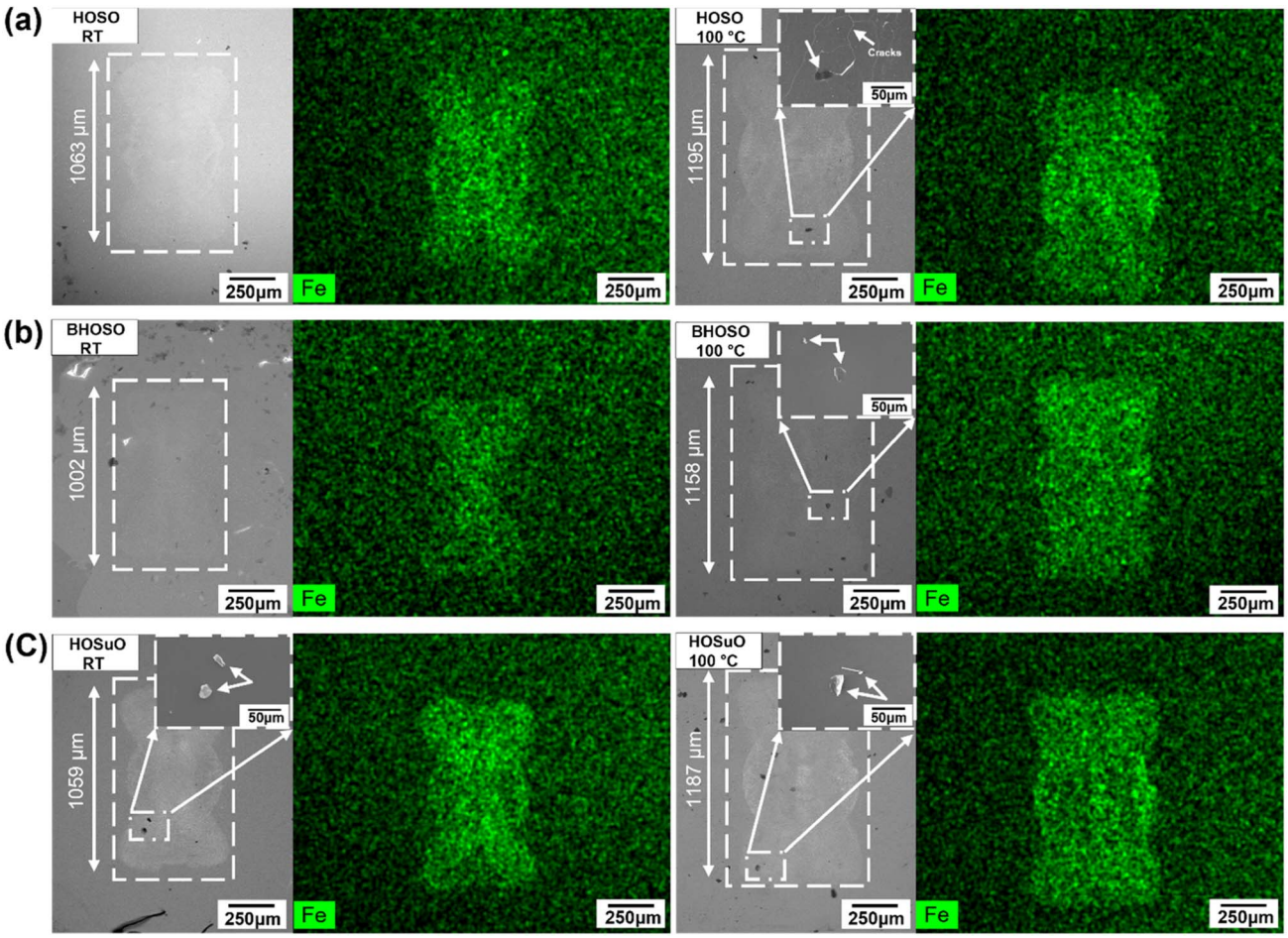

Fig. 11 SEM and EDS images of silicon nitride balls at room and high temperature (a) HOSO, (b) BHOSO and (c) HOSuO. Representative images showing the morphology and mechanism of wear on the surface of the balls after the sliding tests.

signal) from the flat (steel) to ball (Si_3N_4) during the experiments and the formation of a tribo-oxide layer, identified as an iron oxide, which covered the entire worn surface. This iron oxide layer was formed due to the transfer of iron (Fe) from the flat samples to the ball surface, which implied that adhesion is the dominant wear mechanism for the balls used at both temperature levels and in all three lubricated cases. Adhesion wear refers to the process where two surfaces slide against each other, resulting in the transfer of material from one surface to another. This transfer occurs due to the formation and subsequent rupture of atomic bonds between the surfaces.[65,72] As the wear progressed, there is a possibility of localized accumulation of worn-out particles which eventually got detached from the flat surfaces. Point EDS analysis (Fig. S2‡) on select worn out particles (marked with an arrow in Fig. 11) confirmed that these were composed solely of silicon and oxygen, indicating that they were generated primarily from Si_3N_4 balls. The black circular regions in BSE micrographs were primarily small size pitted regions due to the chemical reaction between lubricants and test surfaces, and the presence of foreign elements was not observed in these regions.[73] HOSO lubricated silicon nitride balls at high temperature (Fig. 11a) showed significant pitting surrounded by crack networks at high temperature. The lengths of the worn-out surfaces were 1063 μm and 1195 μm at room and high temperature, respectively. In contrast, Fig. 11b confirms that the BHOSO lubricated ball surface experienced comparatively enhanced surface protection resulting in the least wear track length with no visible cracks. Fig. 11(c) shows the topography of a HOSuO lubricated worn-out silicon nitride ball where the size of the worn-out particles was higher than that in HOSO and BHOSO lubricated cases, which was observed under both temperature conditions. Moreover, a rod-like structure was visualized at high temperatures as marked in Fig. 11c which are potentially hydroxylated silicon oxide rolls as reported by Dong *et al.*[74] and Dante *et al.*[75]

5. Conclusion

A new chemical process was utilized to modify high oleic soybean oil (HOSO), and its tribological behavior was investigated and compared against that of raw HOSO and high oleic sunflower oil. The key findings are summarized below:

- The high oleic soybean oil was successfully chemically modified by adding an isopropyl group to the triglyceride's unsaturated fatty acid components. Such chemical modification impacted its physicochemical properties significantly. In particular, the kinematic viscosity at 40 °C of BHOSO became 4 times higher than that of HOSO. Higher viscosity of BHOSO can be attributed to the presence of an alkyl branch, which impedes the flow of molecules. BHOSO displayed higher oxidation peak temperature (PT) values indicating increased oxidation stability which is one of the major challenges in biolubricants. An increase in PT, along with a decrease in the cloud point presents great potential of this modified lubricant for low temperature applications. The lower pour point properties of HOSO and BHOSO in comparison to HOSuO may result from the higher saturation levels in their compositions.
- BHOSO showed the highest coefficient of friction, followed by HOSuO and HOSO. At room temp, BHOSO had a 22.8% higher COF than HOSO; at 100 °C; it increased by 18.5%. This is due to branching in the molecular structure, resulting in an irregular molecular shape along with increased viscosity. BHOSO exhibited the highest wear resistance among the three lubricants, with wear volumes 10.6% and 10.7% lower than those of HOSO under normal and high-temperature conditions, respectively. This could be due to the presence of less unsaturated fatty acids in BHOSO than in HOSO resulting in better thermo-oxidative characteristics along with better surface protection due to increased viscosity. HOSuO had a slightly higher wear volume than HOSO, which can be attributed to the higher amount of polyunsaturated fatty acids in HOSuO.
- No transferred material was visible in any of the flat wear tracks, and abrasive wear was the primary wear mechanism under room and high-temperature conditions. Dislodged metal flakes or spalling was observed under all three lubrication conditions. Corrosion induced pits were observed inside wear tracks under both temperature conditions. Unlike flat samples, adhesive wear was the primary wear mechanism for the ball surfaces. The formation of an iron oxide layer on the worn surface was identified, which is attributed to the transfer of iron from flat samples to the ball surface during experiments.

Conflicts of interest

There is no conflicts to declare.

Acknowledgements

The authors express their gratitude to the North Dakota Soybean Council for generously providing the funding that supported the research endeavors. Special acknowledgment is extended to Jay Evenstad from the University of North Dakota for his invaluable assistance in the fabrication of the sample holder for the tribological testing. The authors extend their gratitude to Michael J. Powell for viscosity and density analyses.

References

1 W. Qin, M. Wang, W. Sun, P. Shipway and X. Li, Modeling the effectiveness of oil lubrication in reducing both friction and wear in a fretting contact, *Wear*, 2019, **426–427**, 770–777, DOI: 10.1016/j.wear.2019.02.029.
2 R. S. Kamal, N. S. Ahmed and A. M. Nasser, Study the efficiency of some compounds as lubricating oil additives, *Appl. Petrochem. Res.*, 2013, **3**(1–2), 1–8, DOI: 10.1007/s13203-012-0020-8.
3 I. Shodji Tamada, P. Renato, M. Lopes, R. N. Montagnolli and E. D. Bidoia, Biodegradation and Toxicological Evaluation of Lubricant Oils, *Arch. Biol. Technol. v*, **55**(6), 951–956.
4 R. vazquez-duhalt, *Environmental Impact of Used Motor Oil*, 1989.
5 W. J. Bartz, *Lubricants and the Environment*, 1998.

6 F. Ed Erique Haus, J. German, and G.-A. Junter, *Primary Biodegradability of Mineral Base Oils in Relation to Their Chemical and Physical Characteristics*, **https://www.elsevier.com/locate/chemosphere**.
7 C. J. Reeves, A. Siddaiah and P. L. Menezes, Ionic Liquids: A Plausible Future of Bio-lubricants, *J. Bio- Tribo-Corros.*, 2017, **3**(2), DOI: **10.1007/s40735-017-0076-1**.
8 M. Höök and X. Tang, Depletion of fossil fuels and anthropogenic climate change-A review, *Energy Policy*, 2013, **52**, 797–809, DOI: **10.1016/j.enpol.2012.10.046**.
9 W. Liu, K. Wang, J. Song, L. Zhang and Y. Liu, Ultralow friction of basil-based gel in the presence of ethanol as a green lubricant for biomedical applications, *Tribol. Int.*, 2022, **165**, 107320, DOI: **10.1016/j.triboint.2021.107320**.
10 V. Kharka, N. K. Jain and K. Gupta, Performance comparison of green lubricants in gear hobbing with minimum quantity lubrication, *Tribol. Int.*, 2022, **173**, 107582, DOI: **10.1016/j.triboint.2022.107582**.
11 X. Cui, N. Sun, P. Cao, J. Guo and P. Ming, Preparation and application of sustainable nanofluid lubricant from waste soybean oil and waste serpentine for green intermittent machining process, *J. Manuf. Process.*, 2022, **77**, 508–524, DOI: **10.1016/j.jmapro.2022.03.032**.
12 B. K. Sharma, J. M. Perez and S. Z. Erhan, Soybean oil-based lubricants: A search for synergistic antioxidants, *Energy Fuels.*, 2007, **21**(4), 2408–2414, DOI: **10.1021/ef0605854**.
13 H. O. Yosief, M. I. Sarker, G. B. Bantchev, R. O. Dunn and S. C. Cermak, Physico-chemical and tribological properties of isopropyl-branched chicken fat, *Fuel*, 2022, **316**, 123293, DOI: **10.1016/j.fuel.2022.123293**.
14 N. Sapawe, M. Farhan Hanafi, and S. Samion, *The Use of Palm Oil as New Alternative Biolubricant for Improving Anti-friction and Anti-wear Properties*, 2019, **https://www.sciencedirect.comwww.materialstoday.com/proceedings2214-7853**.
15 N. A. Zainal, N. W. M. Zulkifli, M. Gulzar and H. H. Masjuki, A review on the chemistry, production, and technological potential of bio-based lubricants, *Renewable Sustainable Energy Rev.*, 2018, **82**, 80–102, DOI: **10.1016/j.rser.2017.09.004**.
16 J. K. Mannekote, S. V. Kailas, K. Venkatesh and N. Kathyayini, Environmentally friendly functional fluids from renewable and sustainable sources-A review, *Renewable Sustainable Energy Rev.*, 2018, **81**, 1787–1801, DOI: **10.1016/j.rser.2017.05.274**.
17 H. L. Fang and R. L. Mccormick, *Spectroscopic Study of Biodiesel Degradation Pathways*, 2006.
18 A. Adhvaryu, Z. Liu and S. Z. Erhan, Synthesis of novel alkoxylated triacylglycerols and their lubricant base oil properties, *Ind. Crops Prod.*, 2005, **21**(1), 113–119, DOI: **10.1016/j.indcrop.2004.02.001**.
19 N. Kumar, Oxidative stability of biodiesel: Causes, effects and prevention, *Fuel*, 2017, **190**, 328–350, DOI: **10.1016/j.fuel.2016.11.001**.
20 M. P. Schneider, Plant-oil-based lubricants and hydraulic fluids, *J. Sci. Food Agric.*, 2006, **86**(12), 1769–1780, DOI: **10.1002/jsfa.2559**.
21 N. H. Jayadas, K. Prabhakaran Nair and A. G, Tribological evaluation of coconut oil as an environment-friendly lubricant, *Tribol. Int.*, 2007, **40**(2), 350–354, DOI: **10.1016/j.triboint.2005.09.021**.
22 A. Ruggiero, R. D'Amato, M. Merola, P. Valašek and M. Müller, Tribological characterization of vegetal lubricants: Comparative experimental investigation on Jatropha curcas L. oil, Rapeseed Methyl Ester oil, Hydrotreated Rapeseed oil, *Tribol. Int.*, 2017, **109**, 529–540, DOI: **10.1016/j.triboint.2017.01.030**.
23 N. Talib, R. M. Nasir and E. A. Rahim, Tribological behaviour of modified jatropha oil by mixing hexagonal boron nitride nanoparticles as a bio-based lubricant for machining processes, *J. Cleaner Prod.*, 2017, **147**, 360–378, DOI: **10.1016/j.jclepro.2017.01.086**.
24 T. Ouyang, W. Lei, W. Tang, Y. Shen and C. Mo, Experimental investigation of the effect of IF-WS2 as an additive in castor oil on tribological property, *Wear*, 2021, **486–487**, 204070, DOI: **10.1016/j.wear.2021.204070**.
25 C. J. Reeves and P. L. Menezes, Evaluation of boron nitride particles on the tribological performance of avocado and canola oil for energy conservation and sustainability, *Int. J. Adv. Manuf. Technol.*, 2017, **89**(9–12), 3475–3486, DOI: **10.1007/s00170-016-9354-1**.
26 C. Zhao, Y. Jiao, Y. K. Chen and G. Ren, The Tribological Properties of Zinc Borate Ultrafine Powder as a Lubricant Additive in Sunflower Oil, *Tribol. Trans.*, 2014, **57**(3), 425–434, DOI: **10.1080/10402004.2013.878776**.
27 M. T. Siniawski, N. Saniei, B. Adhikari and L. A. Doezema, Influence of fatty acid composition on the tribological performance of two vegetable-based lubricants, *J. Synth. Lubr.*, 2007, **24**(2), 101–110, DOI: **10.1002/jsl.32**.
28 H. H. Masjuki, M. A. Maleque, A. Kubo, and T. Nonaka, *Palm Oil and Mineral Oil Based Lubricants-Their Tribological and Emission Performance*, 1999, **https://www.elsevier.com/locate/triboint**.
29 U. Azzena, *et al.*, Recovery, Purification, Analysis and Chemical Modification of a Waste Cooking Oil, *Waste Biomass Valorization*, 2023, **14**(1), 145–157, DOI: **10.1007/s12649-022-01845-3**.
30 A. Mannu, S. Garroni, J. I. Porras and A. Mele, Available technologies and materials for waste cooking oil recycling, *Processes*, 2020, **8**(3), 366, DOI: **10.3390/PR8030366**.
31 B. Wilson, Lubricants and functional fluids from renewable sources, *Ind. Lubr. Tribol.*, 1998, **50**(1), 6–15, DOI: **10.1108/00368799810781274**.
32 A. Adhvaryu and S. Z. Erhan, *Epoxidized Soybean Oil as a Potential Source of High-Temperature Lubricants*, 2002, **https://www.elsevier.com**.
33 A. Bahari, R. Lewis and T. Slatter, Friction and Wear Phenomena of Vegetable Oil–Based Lubricants with Additives at Severe Sliding Wear Conditions, *Tribol. Trans.*, 2018, **61**(2), 207–219, DOI: **10.1080/10402004.2017.1290858**.
34 N. H. A. Ameen and E. Durak, Study of the tribological properties the mixture of soybean oil and used (waste) frying oil fatty acid methyl ester under boundary

lubrication conditions, *Renew Energy*, 2020, **145**, 1730–1747, DOI: 10.1016/j.renene.2019.06.117.

35 A. Adhvaryu, S. Z. Erhan and J. M. Perez, Tribological studies of thermally and chemically modified vegetable oils for use as environmentally friendly lubricants, *Wear*, 2004, **257**(3–4), 359–367, DOI: 10.1016/j.wear.2004.01.005.

36 R. Kumar and R. K. Gautam, Tribological investigation of sunflower and soybean oil with metal oxide nanoadditives, *Biomass Convers. Biorefin.*, 2022, **14**, 2389–2401, DOI: 10.1007/s13399-022-02411-6.

37 S. Roy, Tribology of multifunctional bio-based lubricants, in *Multifunctional Bio-Based Lubricants: Synthesis, Properties and Applications*, 2023. doi: DOI: 10.1088/978-0-7503-3435-8ch3.

38 N. Ravasio, *et al.*, *Environmental Friendly Lubricants through Selective Hydrogenation of Rapeseed Oil over Supported Copper Catalysts*, 2002.

39 B. Shomchoam and B. Yoosuk, Eco-friendly lubricant by partial hydrogenation of palm oil over Pd/γ-Al2O3 catalyst, *Ind. Crops Prod.*, 2014, **62**, 395–399, DOI: 10.1016/j.indcrop.2014.09.022.

40 U. Biermann and J. O. Metzger, Alkyl-Branched Fatty Compounds: Hydro-Alkylation of Non-Activated Alkenes With Haloalkanes Mediated by Ethylaluminum Sesquichloride, *Eur. J. Lipid Sci. Technol.*, 2018, **120**(1), 1700318, DOI: 10.1002/ejlt.201700318.

41 H. O. Yosief, M. I. Sarker, G. B. Bantchev, R. O. Dunn and S. C. Cermak, Chemical Modification of Beef Tallow for Lubricant Application, *Ind. Eng. Chem. Res.*, 2022, **61**(27), 9889–9900, DOI: 10.1021/acs.iecr.2c01207.

42 F. He, G. Xie and J. Luo, Electrical bearing failures in electric vehicles, *Friction*, 2020, **8**(1), 4–28, DOI: 10.1007/s40544-019-0356-5.

43 H. K. D. H. Bhadeshia, Steels for bearings, *Prog. Mater. Sci.*, 2012, **57**(2), 268–435, DOI: 10.1016/j.pmatsci.2011.06.002.

44 R. Raga, I. Khader, Z. Chlup and A. Kailer, Damage initiation and evolution in silicon nitride under non-conforming lubricated hybrid rolling contact, *Wear*, 2016, **360–361**, 147–159, DOI: 10.1016/j.wear.2016.05.005.

45 V. Brizmer, A. Gabelli, C. Vieillard and G. E. Morales-Espejel, An Experimental and Theoretical Study of Hybrid Bearing Micropitting Performance under Reduced Lubrication, *Tribol. Trans.*, 2015, **58**(5), 829–835, DOI: 10.1080/10402004.2015.1021944.

46 H. O. Yosief, M. I. Sarker, G. B. Bantchev and R. O. Dunn, Isopropyl-branched lard and its potential application as a bio-based lubricant, *Lubr. Sci.*, 2023, DOI: 10.1002/ls.1673.

47 Standard Test Method for Dynamic Viscosity and Density of Liquids by Stabinger Viscometer (and the Calculation of Kinematic Viscosity), DOI: 10.1520/D7042-21.

48 Standard Test Method for Density, Relative Density, and API Gravity of Liquids by Digital Density Meter, DOI: 10.1520/D4052-18A.

49 Standard Practice for Calculating Viscosity Index from Kinematic Viscosity at 40 °C and 100 °C, DOI: 10.1520/D2270-10R16.

50 G. E. Napolitano, Y. Ye and C. Cruz-Hernandez, Chemical Characterization of a High-Oleic Soybean Oil, *J. Am. Oil Chem. Soc.*, 2018, **95**(5), 583–589, DOI: 10.1002/aocs.12049.

51 C. M. Seppanen, Q. Song and A. Saari Csallany, The antioxidant functions of tocopherol and tocotrienol homologues in oils, fats, and food systems, *J. Am. Oil Chem. Soc.*, 2010, **87**(5), 469–481, DOI: 10.1007/s11746-009-1526-9.

52 S. N. Sahasrabudhe, V. Rodriguez-Martinez, M. O'Meara and B. E. Farkas, Density, viscosity, and surface tension of five vegetable oils at elevated temperatures: Measurement and modeling, *Int. J. Food Prop.*, 2017, **20**, 1965–1981, DOI: 10.1080/10942912.2017.1360905.

53 A. Martini, U. S. Ramasamy and M. Len, Review of Viscosity Modifier Lubricant Additives, *Tribol. Lett.*, 2018, **66**(2), 58, DOI: 10.1007/s11249-018-1007-0.

54 E. G. Giakoumis and C. K. Sarakatsanis, Estimation of biodiesel cetane number, density, kinematic viscosity and heating values from its fatty acid weight composition, *Fuel*, 2018, **222**, 574–585, DOI: 10.1016/j.fuel.2018.02.187.

55 I. K. Hong, G. S. Jeon and S. B. Lee, Prediction of biodiesel fuel properties from fatty acid alkyl ester, *J. Ind. Eng. Chem.*, 2014, **20**(4), 2348–2353, DOI: 10.1016/j.jiec.2013.10.011.

56 N. H. Jayadas and K. P. Nair, Coconut oil as base oil for industrial lubricants-evaluation and modification of thermal, oxidative and low temperature properties, *Tribol. Int.*, 2006, **39**(9), 873–878, DOI: 10.1016/j.triboint.2005.06.006.

57 R. D. Lanjekar and D. Deshmukh, A review of the effect of the composition of biodiesel on NO*x* emission, oxidative stability and cold flow properties, *Renewable Sustainable Energy Rev.*, 2016, **54**, 1401–1411, DOI: 10.1016/j.rser.2015.10.034.

58 J. Zhang, A. Tan and H. Spikes, Effect of Base Oil Structure on Elastohydrodynamic Friction, *Tribol. Lett.*, 2017, **65**(1), 13, DOI: 10.1007/s11249-016-0791-7.

59 K.-H. Hentschel Bayer, *The Influence of Molecular Structure on the Frictional Behaviour of Lubricating Fluids*, 1985.

60 W. Hirst and A. J. Moore, Elastohydrodynamic lubrication at high pressures – 2. non-newtonian behavior, *Proc. R. Soc. London, Ser. A*, 1979, **365**(1723), 537–565, DOI: 10.1098/rspa.1979.0033.

61 M. Muraki, *Molecular structure of synthetic hydrocarbon oils and their rheological properties governing traction characteristics*, 1987.

62 C. J. Reeves, P. L. Menezes, T. C. Jen and M. R. Lovell, The influence of fatty acids on tribological and thermal properties of natural oils as sustainable biolubricants, *Tribol. Int.*, 2015, **90**, 123–134, DOI: 10.1016/j.triboint.2015.04.021.

63 N. K. Attia, S. A. El-Mekkawi, O. A. Elardy and E. A. Abdelkader, Chemical and rheological assessment of produced biolubricants from different vegetable oils, *Fuel*, 2020, **271**, 117578, DOI: 10.1016/j.fuel.2020.117578.

64 N. J. Fox, B. Tyrer, and G. W. Stachowiak, *Boundary lubrication performance of free fatty acids in sunflower oil*, 2004.
65 S. Saha and S. Roy, Metallic Dental Implants Wear Mechanisms, Materials, and Manufacturing Processes: A Literature Review, *Materials*, 2023, **16**(1), 161, DOI: **10.3390/ma16010161**.
66 S. Roy and S. Sundararajan, The effect of heat treatment routes on the retained austenite and Tribomechanical properties of carburized AISI 8620 steel, *Surf. Coat. Technol.*, **308**, 236–243, DOI: **10.1016/j.surfcoat.2016.06.095**.
67 P. F. Wang and Z. Han, Friction and wear behaviors of a gradient nano-grained AISI 316L stainless steel under dry and oil-lubricated conditions, *J. Mater. Sci. Technol.*, 2018, **34**(10), 1835–1842, DOI: **10.1016/j.jmst.2018.01.013**.
68 M. T. Siniawski, N. Saniei, B. Adhikari and L. A. Doezema, Influence of fatty acid composition on the tribological performance of two vegetable-based lubricants, *J. Synth. Lubr.*, 2007, **24**(2), 101–110, DOI: **10.1002/jsl.32**.
69 A. Adhvaryu, S. Z. Erhan and J. M. Perez, Tribological studies of thermally and chemically modified vegetable oils for use as environmentally friendly lubricants, *Wear*, 2004, **257**(3–4), 359–367, DOI: **10.1016/j.wear.2004.01.005**.
70 Z. Xu, Z. Lu, J. Zhang, D. Li, J. Liu and C. Lin, The Friction and Wear Behaviours of Inconel 718 Superalloys at Elevated Temperature, *Front. Mater.*, 2021, **8**, DOI: **10.3389/fmats.2021.794701**.
71 S. Roy, N. Sridharan, E. Cakmak, H. Ghaednia, A. Gangopadhyay and J. Qu, Post weld heat treatment and operating temperature effect on tribological behavior of laser cladded stellite 21 coating, *Wear*, 2021, **482–483**, 203990, DOI: **10.1016/j.wear.2021.203990**.
72 H. Choi and S. Roy, Investigating the effect of operating temperature on the tribo-mechanical behavior of cold rolled superelastic nickel titanium alloy, *Wear*, 2023, **523**, 204729, DOI: **10.1016/j.wear.2023.204729**.
73 L. Wang, et al., The effect of tungsten introduction on the tribological properties of Si3N4 ceramics paired with GCr15 steel under nonlubricated conditions, *Wear*, 2022, **506–507**, 204452, DOI: **10.1016/j.wear.2022.204452**.
74 X. Dong and S. Jahanmir, *Wear Transition Diagram for Silicon Nitride*, 1993.
75 R. C. Dante and C. K. Kajdas, A review and a fundamental theory of silicon nitride tribochemistry, *Wear*, 2012, **288**, 27–38, DOI: **10.1016/j.wear.2012.03.001**.